A Cell-Type-Specific Defect in Assembly of Influenza A Virus Particles in Primary Human Macrophages

Sukhmani Bedi and Akira Ono*

Department of Microbiology and Immunology, University of Michigan Medical School, Ann Arbor, MI 48109, USA

* Corresponding Author:

Akira Ono, Ph.D.

Department of Microbiology and Immunology

University of Michigan Medical School

5736 Medical Science Building II, 1150 W. Medical Center Drive

Ann Arbor, MI 48109-0620

Email: akiraono@umich.edu

Abstract:

The primary target of Influenza A virus (IAV) is epithelial cells in the respiratory tract. In contrast to epithelial cells, productive virus infection of most IAV strains is either completely blocked or highly inefficient in macrophages. The exact nature of the defect in IAV replication that leads to inefficient production of progeny virus particles in human macrophages remains to be determined. In this study, we showed that primary human monocyte-derived macrophages (MDM) are inefficient in IAV release even when compared to a macrophage-like cell line, despite comparable levels of viral protein translation and expression of viral glycoproteins at the plasma membrane. Correlative fluorescence scanning electron microscopy revealed that formation of budding structures at the cell surface is inefficient in MDM even though clustering of a viral glycoprotein, hemagglutinin (HA), is observed, suggesting that a step in the assembly process is blocked in this cell type. Using an *in situ* proximity ligation assay, we further determined that association between HA and the viral ion channel protein M2 is defective in MDM. In contrast, HA and another glycoprotein neuraminidase (NA) associate with each other on the MDM surface efficiently. Altogether, our study shows that association between HA with M2 on the plasma membrane is a discrete step in the IAV assembly process, which is separable from the association between HA with NA. Overall, our study lends key insights into cell-type-specific molecular events important for completion of IAV assembly in host cells.

Importance: Viruses rely on host cell factors for efficient replication. Therefore, modulating the interaction between viruses and such host factors is potentially an important therapeutic strategy for blocking virus replication. Identification of host cell determinants important for replication of several viruses has been aided by the discovery of target host cells that possess inherent blocks in viral replication. In this study, we show that primary human MDM are not permissive to IAV replication due to a defect at

the virus particle formation step. This defect is specific to primary human macrophages, since a human monocyte-derived cell line differentiated into macrophage-like morphology supports IAV particle formation. Further, comparison of these cell types suggests that the defect in virus particle assembly in MDM is at least partly due to inefficient association between two viral glycoproteins, HA and M2, on the surface of these cells. Overall, by identifying the viral protein interaction susceptible to cell-type-specific differences, our study suggests the possibility that the interactions between viral components can be targeted to block IAV assembly in infected cells.

54 **Introduction:**

55 Influenza A virus (IAV) is a negative strand RNA virus that mainly infects and
56 replicates in epithelial cells in the respiratory tract. However, the virus has also been
57 shown to infect other cell types such as macrophages, dendritic cells, and mast cells *ex*
58 *vivo*[1-3]. Cell-type-specific differences have been observed for various properties of IAV
59 such as morphology and virulence[4,5]. These differences could be due to differences in
60 expression levels or functions of host cellular proteins between cell types. Previous
61 studies have identified multiple host factors involved in IAV life cycle using genome-wide
62 approaches[6-13]. A complementary approach towards identification of host factors is via
63 comparison between permissive and non-permissive cell types. This approach in which
64 the specific function of the host factor of interest is often determined prior to the identity
65 of the factor has led to identification of virus receptors as well as host factors that restrict
66 replication of viruses[14-17].

67 *Ex vivo* infection studies have shown that in comparison to epithelial cells, murine
68 and human macrophages are less permissive or non-permissive to replication of
69 seasonal virus strains[18-24]. Murine macrophages are non-permissive to seasonal IAV
70 strains[18,20,24,25]. In contrast, primary human blood-derived or alveolar macrophages
71 support seasonal IAV replication at detectable levels although they are still much less
72 permissive to virus growth than human epithelial cells[19,21,22,25]. As for the defective
73 stages of the IAV life cycle, a defect at the entry stage of infection has been identified in
74 murine macrophages for most H1N1 strains[18,20,24]. In addition, other studies have
75 identified a defect(s) at a post-entry stage, either prior to protein translation or at
76 assembly/budding in murine macrophages[20,24]; however, the mechanism in either case
77 has yet to be determined. In contrast to murine macrophages, human macrophages
78 support early stages of replication of all tested IAV strains yet are unable to complete the
79 virus life cycle[24]. While the defect appears to be post-translational, the exact nature of

80 this defect in human macrophages and the molecular mechanism behind it are not
81 known.
82 Determining the exact nature of the human macrophage-specific defect in IAV
83 replication is likely to facilitate identification of human host factors that regulate the IAV
84 life cycle. In the current study, we used primary human MDM in order to identify the
85 defective step in IAV replication in human macrophages. We show that MDM support
86 early stages of the IAV assembly process, i.e. trafficking of the viral glycoproteins
87 hemagglutinin (HA), neuraminidase (NA), and the ion channel protein M2 to the plasma
88 membrane, but are inefficient at virus particle formation and subsequent virus release.
89 This defect in virus particle formation and release is specific to primary MDM, since a
90 monocytic cell line differentiated into macrophage-like cells supports efficient virus
91 particle production. Notably, we observed that the association of HA with M2 on the
92 plasma membrane is highly inefficient in MDM relative to the macrophage-like cells. In
93 contrast, HA and NA associate efficiently on the surface of MDM. Overall, we have
94 identified that virus particle formation, more specifically association between HA and M2,
95 is the defective step in IAV life cycle in primary human macrophages. Our study further
96 showed that association between plasma membrane-localized HA and M2 is a discrete
97 step in IAV assembly, which is regulated by a cell-type-specific factor(s).
98
99

100 **Materials and methods:**

101 **Cells and antibodies:** Madin-Darby canine kidney (MDCK) cells were provided by Dr.
102 Arnold S. Monto (University of Michigan) and were cultured in DMEM (Gibco)
103 supplemented with 10% fetal bovine serum (FBS, Hyclone) and 25 mM HEPES. Human
104 lung carcinoma cell line A549 was provided by Dr. Mike Bachman (University of
105 Michigan) and was cultured in DMEM (Gibco) supplemented with 10% FBS and 25 mM
106 HEPES. Human embryonic kidney-derived 293T cell line (ATCC) was cultured and
107 maintained in DMEM (Lonza) supplemented with 10% FBS. Monocytes were isolated by
108 plate adhesion from peripheral blood mononuclear cells, which were obtained from buffy
109 coats derived from unidentified healthy donors (New York Blood Center, NY). Cells were
110 cultured in RPMI 1640(Gibco) supplemented with 10% FBS for 7 days before they were
111 used for experiments. THP1 (ATCC® TIB202™) cells were cultured in RPMI 1640
112 supplemented with 10% FBS, 1 mM Sodium Pyruvate (Gibco) and 0.05
113 mM 2-mercaptoethanol. To generate differentiated THP1 cells (dTHP1), THP1 cells
114 were cultured in the medium containing 0.1 μM phorbol 12-myristate 12-acetate (PMA;
115 Sigma) and 0.1 μM Vitamin D3 (Sigma) for 2-3 days.
116 The following antibodies were used for immunofluorescence: mouse anti-HA monoclonal
117 antibody (clone C179[26]; Takara), mouse anti-M2 monoclonal antibody (clone 14C2[27];
118 Thermofisher), mouse anti-vRNP monoclonal antibody (clone 61A5[28]; kind gift from Dr.
119 Momose, Kitasato University), goat anti-HA serum (BEI NR-3148), mouse anti-
120 transferrin receptor (TfR) monoclonal antibody (clone M-A712; BD Biosciences).
121 Rabbit anti-NA serum was a kind gift from Dr. Christopher Brooke (University of Illinois).
122 All secondary antibodies used for immunofluorescence were purchased from
123 Thermofisher.
124

125 **Plasmids and virus stocks:** A/WSN/1933 (H1N1) virus was generated by reverse
126 genetics[29]. WSN virus was rescued following transfection of 293T cells with the 8 pPolI
127 plasmids and the 4 pCAGGS plasmids (encoding the PA, PB1, PB2, and NP proteins)
128 using TransIT-293 transfection reagent (Mirus). Forty-eight hours post transfection, virus
129 supernatant from 293T cells was collected and propagated in MDCK cells for 48-72
130 hours. Virus titers of propagated WSN virus were determined using the plaque assay
131 with MDCK cells, and the virus stock was stored at -80°C. A/Wyoming/03/2003 (H3N2)
132 (Wyoming H3N2), A/Panama/2007/1999 (H3N2) (Panama H3N2), and
133 A/California/07/2009 (H1N1) (California H1N1) viruses were a kind gift from Dr. Arnold
134 S. Monto (University of Michigan). All viruses were received as low passage stocks (less
135 than 5 passages in MDCK cells) of virus purified from clinical specimen.
136
137 **Virus infections:** For virus infection, cells were first washed twice with MEM-BSA
138 medium (1X MEM supplemented with 0.3% BSA (Sigma), 0.23% sodium bicarbonate
139 (Gibco), 1X MEM amino acids (Gibco), and 1X MEM vitamins (Gibco)). The cells were
140 then incubated with 200 µl diluted virus for 1 hour at 37°C, washed twice with MEM-
141 BSA, and cultured in MEM-BSA containing 0.2 µg/ml tosylsulfonyl phenylalanyl
142 chloromethyl ketone (TPCK)-treated trypsin (Worthington).
143
144 **Infectious virus measurement by plaque assay:** Confluent monolayers of MDCK cells
145 were washed twice with MEM-BSA and incubated with 100 µl of serial dilutions of virus
146 supernatants for 1 hour at 37°C. Cells were washed once with MEM-BSA and layered
147 with MEM-BSA containing 0.76 ug/ml TPCK-treated trypsin and 1% Seakem GTG
148 agarose /Seaplaque (Lonza) and incubated at 37°C for 48-72 hours. The agarose was
149 removed, and the cells were stained with crystal violet (0.1% crystal violet in 20%
150 methanol) for 10 minutes before counting plaques.

151

152 **Immunostaining and flow cytometry:** For viral protein expression analysis by flow
153 cytometry, virus- or mock-infected cells were detached using 0.06% trypsin-EDTA and
154 fixed with 4% paraformaldehyde (PFA, Electron Microscopy Sciences) in phosphate-
155 buffered saline (PBS) for 20 minutes at room temperature. After fixation, cells were
156 washed twice with 2% FBS in PBS (FACS buffer). For detecting viral protein expression
157 on the cell surface, cells were subsequently incubated with primary antibodies for 45-60
158 minutes directly. For staining of intracellular proteins, cells were first permeabilized with
159 0.1% TritonX-100 in PBS for 5 minutes and then probed with primary antibodies. After
160 washing once with the FACS buffer, cells were incubated with fluorescently labeled
161 secondary antibodies (Invitrogen) for 20-30 minutes. Cells were washed twice with the
162 FACS buffer and analyzed using the FACSCanto flow cytometer (BD Biosciences). Data
163 were analyzed in FlowJo (Treestar) and the positive gates were set using the mock-
164 infected controls.

165

166 **Measurement of vRNA levels:** Virus-containing cell culture supernatants were
167 centrifuged at 3000 rpm for 5 minutes, filtered through a 0.45-μm filter, and subjected to
168 ultracentrifugation at 30,800 rpm (AH650 swinging bucket rotor) for 90 minutes to
169 prepare virus pellets. Virus and cell-associated vRNA was measured using a previously
170 described protocol[30]. Briefly, total RNA was extracted from virus pellets and cell lysates
171 using TRIzol reagent (Ambion) according to the manufacturer's protocol.
172 Complementary DNA was generated using random hexamer priming and the
173 SuperScript III First-Strand Synthesis System (Invitrogen). Quantitative PCR was
174 performed on a CFX96 Real Time PCR system (Biorad) using Platinum SYBR Green
175 pPCR SuperMiX-UDG (Thermo Scientific Fisher) with primers described below. Serial
176 ten-fold dilutions of plasmids containing specific viral gene of WSN were used to

177 generate a standard curve for quantification of cDNA copy number based on cycle
178 threshold (Ct) values. The following primers were used: PB1 forward: 5'-
179 TCAGAGAAAGAGACGAGTGAG-3', PB1 reverse: 5'- AAACCCCCTTATTTGCATCC-3',
180 PB2 forward: 5'- GTTGGGAGAAGAGCAACAGC-3', PB2 reverse: 5'-
181 GATTCGCCCTATTGACGAAA-3', PA forward: 5'- TGTGCAGCAATGGATGATTT-3', PA
182 reverse: 5'- TCTCCCATTTGTGTGGTTCA-3', NP forward: 5'-
183 GCGCCAAGCTAATAATGGTG-3', NP reverse: 5'-GGAGTGCCAGATCATCATGT-3', M
184 forward: 5'-GACCRATCCTGTCACCTCTGAC-3', M reverse: 5'-
185 AGGGCATTYTGGACAAAKCGTCTA-3', NS forward: 5'-
186 CAGAATGGACCAGGCGATCA-3', NS reverse: 5'-TAGAGTCTCCAGCCGGTCAA-3',
187 HA forward: 5'-TAACCTGCTCGAAGACAGAC-3', HA reverse: 5'-
188 AGAGCCATCCGGTGATGTTA-3', NA forward: 5'- TTGGTCAGCAAGTGCATGTC-3',
189 NA reverse: 5'- ACAGCCACTGCTCCATCATC-3'.
190
191 **Correlative fluorescence and scanning electron microscopy (CFSEM):** CFSEM
192 experiments were performed as described before[31]. Briefly, cells cultured on gridded
193 coverslips (Bellco Biotechnology) were infected with WSN at MOI 0.1. Cells were fixed
194 with 4% PFA in PBS at 20-24 hpi. Cells were then rinsed in PBS, and the remaining PFA
195 was quenched by incubating the cells in PBS containing 0.1 M glycine (Sigma) in PBS
196 for 10 min. Cells were blocked by incubation in PBS containing 3% bovine serum
197 albumin (BSA, Sigma) in PBS for 20 minutes. After blocking, cells were stained with
198 mouse anti-HA primary antibody for 45-60 minutes, followed by incubation with
199 fluorescently labeled secondary antibody. Cells were then washed in PBS and imaged
200 using a Leica Inverted SP5X Confocal Microscope with a 40× PL APO objective and 10-
201 20× scanning zoom. After fluorescence imaging, cells were fixed with PBS containing
202 2.5% glutaraldehyde (Electron Microscopy Sciences) at 4°C overnight. Cells were then

203 rinsed with Sorenson's buffer (0.1 M sodium phosphate buffer, pH 7.4), stained with 1%
204 OsO_4 in Sorenson's buffer for 30 min, rinsed again in Sorenson's buffer, and then
205 dehydrated in a series of 10-min ethanol washes at 30%, 50%, 70%, 90%, 100%, and
206 100% (vol/vol in water). Cells were then rinsed twice for 15 min each in
207 hexamethyldisilazane (Electron Microscopy Sciences) and allowed to dry overnight.
208 After dehydration, coverslips were affixed to specimen mounts and sputter coated with
209 gold for 90 s (Polaron). Cells were identified by their location on the gridded coverslip
210 and imaged on an Amray 1910FEG scanning electron microscope at 5-10 kV. Digital
211 SEM images were collected with an X-Stream Digital Image Capture System (SEMTech
212 Solutions). Fluorescence and SEM images were roughly brought into registration by
213 scaling and rotating images in Adobe Illustrator, similarly to other correlative
214 fluorescence/SEM studies. Landmarks used for registration included cell edges. Cell
215 surface structures visible in SEM were manually classified as virus-like buds if they
216 appeared spherical and near 100 nm in diameter. Number of HA-positive puncta was
217 measured in the fluorescence images using the *Analyze particle* function in ImageJ.
218 Since MDM have microfolds on the cell surface, especially towards the center of the cell,
219 but have a flatter topology towards the edge of the cells, we focused on areas towards
220 the edge of the cells for quantification of efficiency of virus bud formation.
221
222 **Surface protein colocalization analysis:** Virus-infected dTHP1 cells and MDM were
223 washed with PBS and fixed with 4% PFA for 20 minutes. Cells were then blocked with
224 PBS containing 3% BSA for 20 minutes at room temperature. Cells were incubated with
225 anti-HA and anti-M2 primary antibodies for 45-60 minutes at room temperature, washed
226 twice with PBS, and stained with fluorescently labeled secondary antibodies. Cells were
227 subsequently washed with PBS, and slides were mounted with coverslips using
228 Fluoromount G (SouthernBiotech) as mounting medium. Cells were examined using a

229 Leica Inverted SP5X Confocal Microscope System with a 63x or 100X objective.
230 Pearson's correlation coefficients between HA and M2 were calculated using the Coloc2
231 plugin in the ImageJ software program. Eight-ten cells were analyzed per experiment for
232 each condition.
233
234 ***In situ* Proximity Ligation Assay (PLA):** PLA was performed according to
235 Duolink® PLA fluorescence protocol (Sigma). Briefly, WSN-infected dTHP1 cells or MDM
236 were fixed with 4% PFA and blocked with Duolink® PLA Blocking Buffer. Cells were
237 incubated with the following primary antibody combinations: goat anti-HA and mouse
238 anti-M2 for PLA and rabbit anti-NA for identification of infected cells; mouse anti-HA and
239 rabbit anti-NA for PLA and goat anti-HA for identification of infected cells; or goat anti-HA
240 and mouse anti-TfR for PLA and rabbit anti-NA for identification of infected cells. After
241 washing twice with PLA Wash Buffer A, cells were incubated with PLA probes that bind
242 goat and mouse primary antibodies (for HA-M2 and HA-TfR PLA) or mouse and rabbit
243 primary antibodies (for HA-NA PLA). In addition to the PLA probes, the cells were co-
244 stained with a fluorescently labeled secondary antibody recognizing anti-NA (for HA-M2
245 and HA-TfR PLA) or anti-HA (for HA-NA PLA). Probe ligation and amplification steps
246 were carried out according to manufacturer's instructions. After washes, slides were
247 mounted with a cover slip using Duolink® In Situ Mounting Medium. Cells were observed
248 using a Leica Inverted SP5X Confocal Microscope System with a 63X objective. Z-
249 stacks were acquired for each cell, and the maximum intensity projection for each cell
250 was constructed using ImageJ. The projection image was thresholded, and the number
251 of PLA-positive spots was counted using the *Analyze particle* function in ImageJ. Eight-
252 ten cells were analyzed per experiment for each condition.
253
254

255 **Results:**

256

257 **MDM are inefficient in supporting productive IAV infection relative to differentiated**
258 **THP1 cells**

259 To determine the extent to which human epithelial cells and macrophages differ
260 in their ability to support productive IAV infection, we compared infectious IAV release
261 from three different human cell types: the lung-derived epithelial cell line A549, the
262 monocytic cell line THP1, which has been differentiated to adopt macrophage-like
263 morphology (dTHP1), and primary monocyte-derived macrophages (MDM). The dTHP1
264 cells were obtained via treatment of THP1 cells with phorbol 12-myristate 12-acetate
265 (PMA) and Vitamin D3 for 2-3 days. Upon infection with the laboratory strain
266 A/WSN/1933 (H1N1) (WSN) at MOI 0.01, we observed that virus titers in MDM culture
267 supernatants were up to 100-fold reduced in comparison to that in A549 culture
268 supernatants at 11 hours post infection (hpi). Unexpectedly, virus titers in culture
269 supernatants were similar between A549 and dTHP1 cells (Figure 1A). Since dTHP1
270 cells differ from MDM in its ability to support influenza virus replication and yet belong to
271 the same cellular lineage, to facilitate the analyses of MDM-specific defect(s), we chose
272 to compare IAV replication in MDM with that in dTHP1 cells in subsequent experiments.
273 While MDM isolated from the vast majority of the tested human donors (Group 1)
274 showed a defect in productive IAV infection relative to dTHP1 at 24 hpi, MDM from some
275 donors (Group 2; ~20%) showed no significant difference (Figure 1B). Therefore, to
276 identify the MDM-specific defect and its mechanism, the subsequent experiments were
277 performed using MDM from the donors in Group 1.

278 To assess whether other IAV strains also replicate inefficiently in MDM relative to
279 dTHP1 cells, we compared productive infection in dTHP1 cells and MDM of three
280 previously or currently circulating IAV strains, in addition to WSN: A/Wyoming/03/2003

281 (H3N2) [Wyoming (H3N2)], A/Panama/2007/1999 (H3N2) [Panama (H3N2)], and
282 A/California/07/2009 (H1N1) [California (H1N1)]. Infectious virus titers of all tested IAV
283 strains, as measured by the plaque assay, were reduced by 10-50-fold in MDM in
284 comparison to dTHP1 cells (Figure 1C).

285 To determine whether the same number of cells are infected in both dTHP1 and
286 MDM cultures, we compared the percentage of infected cells as well as release of
287 infectious virus particles from dTHP1 cells and MDM at different time points post
288 infection. Upon infection with WSN, Wyoming (H3N2), and Panama (H3N2), we
289 observed a significant reduction in infectious virus production from MDM at 24 hpi or
290 later relative to dTHP1 cells (Figure 2, top panels). The percentage of virus-infected
291 cells, measured using an antibody (61A5) that specifically recognizes nucleoprotein (NP)
292 in complex with viral RNA (vRNP)[28], showed no difference between dTHP1 cells and
293 MDM at different time points with any of the tested viral strains (Figure 2, lower panels).
294 These results suggest that even though the number of IAV-infected cells are similar
295 between dTHP1 cells and MDM, MDM are highly inefficient at producing infectious virus
296 in comparison to dTHP1 cells.

297

298 **Both efficiency of virus release and infectivity of released particles are reduced in**
299 **MDM relative to dTHP1**

300 Our data thus far suggest that infectious virus release is reduced in MDM relative
301 to dTHP1 cells even though similar number of cells are infected. We sought to address
302 whether the reduction in viral titers in MDM culture supernatants is due to a reduction in
303 infectivity of released particles or whether it is due to a reduction in release of physical
304 particles. To this end, we used viral RNA (vRNA) release as a surrogate to measure
305 release of physical particles from dTHP1 cells and MDM. Number of vRNA copies
306 released from MDM were 7-8-fold reduced in comparison to that from dTHP1 cells for all

307 eight vRNA segments. However, there were no significant differences in vRNA levels in
308 cells. vRNA release efficiency was calculated as the ratio of number of vRNA copies in
309 cell culture supernatants to the total number of vRNA copies (cells + supernatant). For
310 all eight vRNA segments, we observed a 5-10-fold reduction in vRNA release efficiency
311 in MDM relative to dTHP1 cells (Figure 3A). This suggests that efficiency of physical viral
312 particle release from MDM is reduced in comparison to that from dTHP1 cells.
313 Importantly, the reduction in vRNA release (7-8-fold) from MDM does not entirely
314 account for reduction in infectious virus release (up to 50-fold) (Figure 3B). The ratio of
315 released vRNA (representing total number of particles) to released PFU (representing
316 infectious virions) was calculated as the infectivity per particle. Infectivity per particle for
317 virus particles released from MDM was 5-6-fold reduced versus that released from
318 dTHP1 cells (Figure 3B). Overall, our data suggest that the total number of virus
319 particles released as well as the infectivity of released virus particles is reduced in MDM
320 relative to dTHP1 cells.
321
322 **Viral protein translation is not defective in MDM relative to dTHP1 cells**
323 Our data in Figure 1B (% vRNP+ cells) show that vRNP can be detected in both dTHP1
324 cells and MDM similarly, suggesting that virus entry is unlikely to be defective in MDM
325 relative to dTHP1 cells. To determine whether MDM are able to express viral proteins as
326 efficiently as dTHP1 cells, we compared the cellular levels of three viral components,
327 vRNP complex, matrix (M1) protein, and hemagglutinin (HA) protein between dTHP1
328 cells and MDM. The sizes of cell populations that express these components were not
329 different between MDM and dTHP1 cells (Figures 4A and 4B). The mean fluorescence
330 intensity (MFI) of staining for the three viral components in infected cell populations was
331 similar between MDM and dTHP1 cells (Figure 4C). These results suggest that the
332 reduction in virus release from MDM is due to a defect in post-translation step(s).

333

334 **Formation of budding structures is inefficient in MDM relative to dTHP1 cells**
335 **despite similar levels of viral glycoprotein expression at the plasma membrane**

336 Virus assembly is initiated by targeting of the glycoproteins HA and NA to the
337 plasma membrane[32-34]. The third transmembrane protein M2 is also recruited to the
338 assembly sites at the plasma membrane and allows for completion of the virus budding
339 process[33,35]. To determine whether trafficking of the three glycoproteins occurs similarly
340 in dTHP1 cells and MDM, we next compared levels of HA, NA and M2 proteins on the
341 surface of WSN-infected cells. We did not observe a major difference in sizes of cell
342 populations with surface expression of any of the three proteins between MDM and
343 dTHP1 cells (Figures 5A and 5B). The MFI of staining for all three viral proteins in
344 infected cell populations was similar between MDM and dTHP1 cells (Figure 5C),
345 indicating that trafficking of viral glycoproteins to the plasma membrane is not defective
346 in MDM.

347 We next asked whether dTHP1 cells and MDM expressing HA on the cell surface
348 support virus particle formation. To this end, we performed correlative fluorescence and
349 scanning electron microscopy (CFSEM) to first identify cells with surface HA expression
350 using fluorescence microscopy and then examine formation of virus particle-like buds on
351 the surface of the same cells using scanning electron microscopy (SEM). HA-positive
352 clusters or puncta, which likely represent sites of virus assembly, were detected on the
353 surface of infected cells after the images were thresholded to remove background signal.
354 Budding structures with a diameter of approximately 100 nm, corresponding to HA-
355 enriched sites, were observed on the surface of WSN-infected dTHP1 cells. No such
356 budding structures were observed on the surface of mock-infected cells. MDM also form
357 virus particle-like buds on the surface in HA-positive cells, albeit the number of buds
358 observed in MDM were lower than in dTHP1 cells (Figure 6A). The number of HA-

359 positive puncta as well as the number of virus particle-like buds were counted within the
360 same area of each cell. Even though MDM showed higher number of HA-positive puncta
361 on the cell surface than dTHP1 cells, the number of virus buds were drastically reduced
362 in MDM relative to dTHP1 cells (Figure 6B). Overall, these results indicate that MDM are
363 inefficient at virus particle assembly/budding despite efficient trafficking of HA, NA and
364 M2 to the plasma membrane.
365
366 **Association between HA and M2 is defective in MDM but not in dTHP1 cells**
367 To compare formation of putative assembly sites (sites co-enriched in HA, NA
368 and M2) between dTHP1 cells and MDM, we first measured the extent of colocalization
369 between HA and M2 on the surface of the two cell types. Both proteins localized on the
370 cell surface, corroborating the flow cytometry data (Figure 5A), and showed a high
371 degree of colocalization in both dTHP1 cells and MDM (Figure 7A). Moreover, Pearson
372 correlation coefficient analysis showed a slightly higher level of cell surface
373 colocalization between HA and M2 in MDM than in dTHP1 cells (Figure 7B). However,
374 due to the limited resolution offered by confocal microscopy (500-700 nm), it is difficult to
375 distinguish between HA- and M2-co-enriched assembly sites (spanning 300-600 nm[33])
376 and free HA and M2 proteins that are present on the plasma membrane but are not
377 associated with assembly sites. To selectively detect HA- and M2- co-enriched assembly
378 sites on the cell surface, we used *in situ* proximity ligation assay (PLA). PLA allows for
379 detection of two proteins localized within 40-nm distance of each other and has been
380 previously used to visualize IAV assembly sites on the plasma membrane[36]. In addition
381 to measuring PLA signal between the given proteins, we also co-stained cells for cell
382 surface NA to identify infected cells. As a negative control, we performed PLA between
383 HA and transferrin receptor (TfR). TfR does not associate with lipid rafts[37], the plasma
384 membrane microdomains associated with IAV assembly sites[33,38]. Infected dTHP1 cells

385 showed high PLA signal for HA-M2 association. In contrast, infected MDM showed very
386 few PLA spots between HA and M2 (Figures 7C and 7D). As expected, no PLA signal
387 was observed between HA and M2 in mock-infected cells or between HA and TfR in
388 infected cells (Figure 7C). In addition, the majority (80-90%) of both surface NA-positive
389 MDM and dTHP1 cells express HA and M2 on their surface (Figure 7E). Therefore, the
390 significant reduction in HA-M2 PLA signal in MDM relative to dTHP1 cells is not due to
391 the lack of expression of HA and/or M2 in NA-positive cells.
392 To determine whether the defect in association between transmembrane proteins
393 in MDM is specific to HA and M2 or whether association between other pairs of viral
394 transmembrane proteins is defective as well, we next measured PLA signal between HA
395 and NA. In this case, to identify infected cells, we co-stained cells for cell surface HA
396 using an antibody different from the one used for PLA. PLA signal between HA and NA
397 was similar for dTHP1 cells and MDM, suggesting that HA and NA associate with each
398 other as efficiently on the surface of MDM as on dTHP1 cells (Figure 8). Overall, our
399 data suggest that association between HA and M2 is specifically impaired in MDM and
400 may lead to incomplete virus assembly in these cells.
401

402 **Discussion:**

403 In a previous study, a post-translational defect in productive IAV infection was
404 observed in human MDM[24]. A similar defect was also reported for murine macrophages
405 in one study[20] but not the other[24]. The exact nature of these defects that lead to
406 inefficient IAV release has not been determined. Here, we have shown that despite
407 efficient trafficking of the viral glycoproteins to the cell surface (Figure 5), infectious virus
408 particle formation at the plasma membrane is inefficient in this cell type (Figures 3 and
409 6). The current study further identified HA-M2 association as a defective step in IAV
410 assembly in MDM (Figure 7). This negative regulation is specific to primary
411 macrophages as macrophage-like cells derived from the THP1 monocytic cell line
412 (dTHP1 cells) support HA-M2 association and efficient IAV production.

413 Previous studies observed strain-specific differences for IAV replication in human
414 macrophages. Some strains such as highly pathogenic H5N1 and pandemic 1918
415 strains can replicate in macrophages albeit at a lower efficiency than in epithelial
416 cells[18,19,22,25]. Marvin *et al.* recently reported that the laboratory strain WSN is able to
417 overcome blocks in IAV replication in human macrophages, while replication of
418 A/California/04/2009 strain is completely blocked[24]. In our study, infectious virus release
419 of any of the tested IAV strains is not completely blocked in MDM although all tested
420 strains released significantly lower titers in MDM than in dTHP1 cells (Figure 1C). At this
421 point, it remains unclear whether the difference observed with non-WSN strains between
422 these studies arose from the use of different strains or different detection or culture
423 methods. Since productive infection of WSN is reduced in MDM in comparison to dTHP1
424 cells as observed for other tested viral strains in our study, we chose to elucidate the
425 mechanism behind the reduction in IAV release using WSN for which antibody reagents
426 are available to us. In our future studies, we plan to determine whether the molecular

427 mechanism behind defective IAV release from MDM is shared among different IAV
428 strains.

429 In addition to identifying the defective step for IAV replication in primary human
430 macrophages, our study also lends key insights into the assembly and budding process
431 of IAV in host cells. IAV is thought to assemble in cholesterol-enriched microdomains, or
432 membrane rafts, of the plasma membrane in host cells[39-41]. HA and NA accumulate at
433 these assembly sites, also known as the budozones, while the third transmembrane
434 protein M2 is suggested to localize at the edge of the budozone[32,35,38,42]. However, the
435 sequence of events leading to recruitment of M2 to the budozone and the mechanism
436 regulating these events remain to be determined. Our PLA data suggest that association
437 between HA and NA likely precedes association between HA and M2. A recent study
438 showed that NA but not M2 accelerates HA trafficking to the apical surface of epithelial
439 cells, presumably through co-trafficking[42]. Therefore, recruitment of M2 to assembly sites
440 enriched in both HA and NA is a discrete step in the IAV assembly process. While PLA
441 revealed the cell-type-specific difference in association between HA and M2 proteins, it
442 does not inform sizes of clusters containing HA (and NA) only, M2 only, or both and
443 ratios of budozone-associated versus free viral protein populations, both of which are
444 indispensable information for further delineating the assembly process in different cell
445 types. Analyses using super-resolution microscopy is underway to address these points.

446 The cytoplasmic domain of M2 comprises of an amphipathic helix, which plays a
447 role in scission of the IAV particle after budding[35,43]. Previous studies have described the
448 role of M2 in assembly and scission of virus buds[35,43], vRNP incorporation[44-46], and M1
449 binding[44,47-49] using virus strains that either lack M2 expression or express cytoplasmic
450 tail mutant versions of the protein. Interestingly, in epithelial cells, virus lacking M2 or
451 expressing mutant M2 proteins is still able to initiate particle assembly and budding,
452 presumably mediated by HA and NA. However, these buds adopt an abnormal

453 morphology and/or fail to undergo scission or release[35,46,50], latter of which results in
454 accumulation of particles at the cell surface. In contrast, MDM show very few buds on
455 their surface (Figure 6), suggesting that in MDM, a role for M2 early in virus particle
456 assembly is more prominent than in epithelial cells. Consistent with this early role of M2
457 in IAV assembly, M2 functions in recruitment of M1 and vRNP to assembly sites, which
458 is important for initiation and/or completion of IAV particle assembly[51-53]. In this case, a
459 cell-type-specific defect in incorporation of M1 and/or vRNP into budding virus particles
460 in MDM may explain the reduction in infectivity per particle observed for MDM-derived
461 virus relative to dTHP1-derived virus (Figure 3B).

462 Alternatively, it is possible that virus particle assembly mediated by HA and NA
463 occurs in macrophages in the absence of M2 association with assembly sites. However,
464 assembling or assembled IAV particles may be sequestered into intracellular
465 compartments as previously observed for HIV-1[54-56]. While HIV-1 assembles at the
466 plasma membrane in T cells and other tested cell lines[57,58], assembling or assembled
467 HIV-1 particles accumulate in intracellular virus containing compartments (VCCs) in
468 macrophages[56,59-63]. We previously observed that multimerization of the HIV-1 structural
469 protein at the plasma membrane promotes its localization to VCC[64]. It is possible that in
470 an analogous manner, assembling IAV particles are quickly sequestered in intracellular
471 compartments in MDM. Such intracellular accumulation is not detectable with CFSEM,
472 which allows for detection of budding structures only on the cell surface. Our future
473 studies will assess using transmission electron microscopy whether assembled or
474 assembling IAV particles accumulates in intracellular compartments in macrophages.

475 Overall, in this study, we have compared IAV replication in MDM with that in
476 dTHP1 cells and found that MDM replicate vRNA, express viral proteins, and traffic HA,
477 NA and M2 to the plasma membrane at levels similar to those in dTHP1. However, MDM
478 are defective in assembling virus particles, likely due impaired association between the

479 viral transmembrane proteins HA and M2. In future studies, identification of all the viral
480 factors involved in inefficient IAV budding and release in MDM will potentially aid in
481 understanding of the host cell mechanisms restricting IAV replication in this cell type. In
482 addition, comparing MDM and dTHP1 cells, which are of the same lineage, will facilitate
483 identification of additional host cellular factors involved in the assembly stage of the IAV
484 life cycle.
485
486 References:
487
488

489 1 Rodgers, B. C. & Mims, C. A. Influenza virus replication in human alveolar
490 macrophages. *J Med Virol* **9**, 177-184 (1982).
491 2 Hartmann, B. M. *et al.* Mouse dendritic cell (DC) influenza virus infectivity is
492 much lower than that for human DCs and is hemagglutinin subtype dependent. *J*
493 *Virol* **87**, 1916-1918, doi:10.1128/JVI.02980-12 (2013).
494 3 Graham, A. C., Hilmer, K. M., Zickovich, J. M. & Obar, J. J. Inflammatory
495 response of mast cells during influenza A virus infection is mediated by active
496 infection and RIG-I signaling. *J Immunol* **190**, 4676-4684,
497 doi:10.4049/jimmunol.1202096 (2013).
498 4 Roberts, P. C. & Compans, R. W. Host cell dependence of viral morphology.
499 *Proc Natl Acad Sci U S A* **95**, 5746-5751 (1998).
500 5 Moncorgé, O., Mura, M. & Barclay, W. S. Evidence for avian and human host cell
501 factors that affect the activity of influenza virus polymerase. *J Virol* **84**, 9978-
502 9986, doi:10.1128/JVI.01134-10 (2010).
503 6 Hao, L. *et al.* Drosophila RNAi screen identifies host genes important for
504 influenza virus replication. *Nature* **454**, 890-893, doi:10.1038/nature07151
505 (2008).
506 7 Shapira, S. D. *et al.* A physical and regulatory map of host-influenza interactions
507 reveals pathways in H1N1 infection. *Cell* **139**, 1255-1267,
508 doi:10.1016/j.cell.2009.12.018 (2009).
509 8 Karlas, A. *et al.* Genome-wide RNAi screen identifies human host factors crucial
510 for influenza virus replication. *Nature* **463**, 818-822, doi:10.1038/nature08760
511 (2010).
512 9 König, R. *et al.* Human host factors required for influenza virus replication. *Nature*
513 **463**, 813-817, doi:10.1038/nature08699 (2010).
514 10 Su, W. C. *et al.* Pooled RNAi screen identifies ubiquitin ligase Itch as crucial for
515 influenza A virus release from the endosome during virus entry. *Proc Natl Acad*
516 *Sci U S A* **110**, 17516-17521, doi:10.1073/pnas.1312374110 (2013).
517 11 Watanabe, T. *et al.* Influenza virus-host interactome screen as a platform for
518 antiviral drug development. *Cell Host Microbe* **16**, 795-805,
519 doi:10.1016/j.chom.2014.11.002 (2014).
520 12 Tripathi, S. *et al.* Meta- and Orthogonal Integration of Influenza "OMICs" Data
521 Defines a Role for UBR4 in Virus Budding. *Cell Host Microbe* **18**, 723-735,
522 doi:10.1016/j.chom.2015.11.002 (2015).

523 13 Meliopoulos, V. A. *et al.* Host gene targets for novel influenza therapies
524 elucidated by high-throughput RNA interference screens. *FASEB J* **26**, 1372-
525 1386, doi:10.1096/fj.11-193466 (2012).
526 14 Laguette, N. *et al.* SAMHD1 is the dendritic- and myeloid-cell-specific HIV-1
527 restriction factor counteracted by Vpx. *Nature* **474**, 654-657,
528 doi:10.1038/nature10117 (2011).
529 15 Perez-Caballero, D. *et al.* Tetherin inhibits HIV-1 release by directly tethering
530 virions to cells. *Cell* **139**, 499-511, doi:10.1016/j.cell.2009.08.039 (2009).
531 16 Sheehy, A. M., Gaddis, N. C., Choi, J. D. & Malim, M. H. Isolation of a human
532 gene that inhibits HIV-1 infection and is suppressed by the viral Vif protein.
533 *Nature* **418**, 646-650, doi:10.1038/nature00939 (2002).
534 17 Neil, S. J., Zang, T. & Bieniasz, P. D. Tetherin inhibits retrovirus release and is
535 antagonized by HIV-1 Vpu. *Nature* **451**, 425-430, doi:10.1038/nature06553
536 (2008).
537 18 Cline, T. D., Karlsson, E. A., Seufzer, B. J. & Schultz-Cherry, S. The
538 hemagglutinin protein of highly pathogenic H5N1 influenza viruses overcomes an
539 early block in the replication cycle to promote productive replication in
540 macrophages. *J Virol* **87**, 1411-1419, doi:10.1128/JVI.02682-12 (2013).
541 19 Yu, W. C. *et al.* Viral replication and innate host responses in primary human
542 alveolar epithelial cells and alveolar macrophages infected with influenza H5N1
543 and H1N1 viruses. *J Virol* **85**, 6844-6855, doi:10.1128/JVI.02200-10 (2011).
544 20 Londrigan, S. L. *et al.* Infection of Mouse Macrophages by Seasonal Influenza
545 Viruses Can Be Restricted at the Level of Virus Entry and at a Late Stage in the
546 Virus Life Cycle. *J Virol* **89**, 12319-12329, doi:10.1128/JVI.01455-15 (2015).
547 21 Mok, C. K., Lee, D. C., Cheung, C. Y., Peiris, M. & Lau, A. S. Differential onset of
548 apoptosis in influenza A virus H5N1- and H1N1-infected human blood
549 macrophages. *J Gen Virol* **88**, 1275-1280, doi:10.1099/vir.0.82423-0 (2007).
550 22 Sakabe, S. *et al.* Cytokine production by primary human macrophages infected
551 with highly pathogenic H5N1 or pandemic H1N1 2009 influenza viruses. *J Gen*
552 *Virol* **92**, 1428-1434, doi:10.1099/vir.0.030346-0 (2011).
553 23 van Riel, D. *et al.* Highly pathogenic avian influenza virus H5N1 infects alveolar
554 macrophages without virus production or excessive TNF-alpha induction. *PLoS*
555 *Pathog* **7**, e1002099, doi:10.1371/journal.ppat.1002099 (2011).
556 24 Marvin, S. A., Russier, M., Huerta, C. T., Russell, C. J. & Schultz-Cherry, S.
557 Influenza overcomes cellular blocks to productively replicate impacting
558 macrophage function. *J Virol*, doi:10.1128/JVI.01417-16 (2016).
559 25 Perrone, L. A., Plowden, J. K., García-Sastre, A., Katz, J. M. & Tumpey, T. M.
560 H5N1 and 1918 pandemic influenza virus infection results in early and excessive
561 infiltration of macrophages and neutrophils in the lungs of mice. *PLoS Pathog* **4**,
562 e1000115, doi:10.1371/journal.ppat.1000115 (2008).
563 26 Okuno, Y., Isegawa, Y., Sasao, F. & Ueda, S. A common neutralizing epitope
564 conserved between the hemagglutinins of influenza A virus H1 and H2 strains. *J*
565 *Virol* **67**, 2552-2558 (1993).
566 27 Zebedee, S. L. & Lamb, R. A. Influenza A virus M2 protein: monoclonal antibody
567 restriction of virus growth and detection of M2 in virions. *J Virol* **62**, 2762-2772
568 (1988).
569 28 Momose, F., Kikuchi, Y., Komase, K. & Morikawa, Y. Visualization of
570 microtubule-mediated transport of influenza viral progeny ribonucleoprotein.
571 *Microbes Infect* **9**, 1422-1433, doi:10.1016/j.micinf.2007.07.007 (2007).
572 29 Neumann, G. *et al.* Generation of influenza A viruses entirely from cloned
573 cDNAs. *Proc Natl Acad Sci U S A* **96**, 9345-9350 (1999).

30 Pauly, M. D. & Lauring, A. S. Effective lethal mutagenesis of influenza virus by three nucleoside analogs. *J Virol* **89**, 3584-3597, doi:10.1128/JVI.03483-14 (2015).
31 Hogue, I. B., Grover, J. R., Soheilian, F., Nagashima, K. & Ono, A. Gag induces the coalescence of clustered lipid rafts and tetraspanin-enriched microdomains at HIV-1 assembly sites on the plasma membrane. *J Virol* **85**, 9749-9766, doi:10.1128/JVI.00743-11 (2011).
32 Chen, B. J., Leser, G. P., Morita, E. & Lamb, R. A. Influenza virus hemagglutinin and neuraminidase, but not the matrix protein, are required for assembly and budding of plasmid-derived virus-like particles. *J Virol* **81**, 7111-7123, doi:10.1128/JVI.00361-07 (2007).
33 Leser, G. P. & Lamb, R. A. Influenza virus assembly and budding in raft-derived microdomains: a quantitative analysis of the surface distribution of HA, NA and M2 proteins. *Virology* **342**, 215-227, doi:10.1016/j.virol.2005.09.049 (2005).
34 Takeda, M., Leser, G. P., Russell, C. J. & Lamb, R. A. Influenza virus hemagglutinin concentrates in lipid raft microdomains for efficient viral fusion. *Proc Natl Acad Sci U S A* **100**, 14610-14617, doi:10.1073/pnas.2235620100 (2003).
35 Rossman, J. S., Jing, X., Leser, G. P. & Lamb, R. A. Influenza virus M2 protein mediates ESCRT-independent membrane scission. *Cell* **142**, 902-913, doi:10.1016/j.cell.2010.08.029 (2010).
36 Kawaguchi, A., Hirohama, M., Harada, Y., Osari, S. & Nagata, K. Influenza Virus Induces Cholesterol-Enriched Endocytic Recycling Compartments for Budozone Formation via Cell Cycle-Independent Centrosome Maturation. *PLoS Pathog* **11**, e1005284, doi:10.1371/journal.ppat.1005284 (2015).
37 Harder, T., Scheiffele, P., Verkade, P. & Simons, K. Lipid domain structure of the plasma membrane revealed by patching of membrane components. *J Cell Biol* **141**, 929-942 (1998).
38 Zhang, J., Pekosz, A. & Lamb, R. A. Influenza virus assembly and lipid raft microdomains: a role for the cytoplasmic tails of the spike glycoproteins. *J Virol* **74**, 4634-4644 (2000).
39 Schmitt, A. P. & Lamb, R. A. Influenza virus assembly and budding at the viral budozone. *Adv Virus Res* **64**, 383-416, doi:10.1016/S0065-3527(05)64012-2 (2005).
40 Veit, M. & Thaa, B. Association of influenza virus proteins with membrane rafts. *Adv Virol* **2011**, 370606, doi:10.1155/2011/370606 (2011).
41 Rossman, J. S. & Lamb, R. A. Influenza virus assembly and budding. *Virology* **411**, 229-236, doi:10.1016/j.virol.2010.12.003 (2011).
42 Ohkura, T., Momose, F., Ichikawa, R., Takeuchi, K. & Morikawa, Y. Influenza A virus hemagglutinin and neuraminidase mutually accelerate their apical targeting through clustering of lipid rafts. *J Virol* **88**, 10039-10055, doi:10.1128/JVI.00586-14 (2014).
43 Roberts, K. L., Leser, G. P., Ma, C. & Lamb, R. A. The amphipathic helix of influenza A virus M2 protein is required for filamentous bud formation and scission of filamentous and spherical particles. *J Virol* **87**, 9973-9982, doi:10.1128/JVI.01363-13 (2013).
44 Grantham, M. L., Stewart, S. M., Lalime, E. N. & Pekosz, A. Tyrosines in the influenza A virus M2 protein cytoplasmic tail are critical for production of infectious virus particles. *J Virol* **84**, 8765-8776, doi:10.1128/JVI.00853-10 (2010).

45 McCown, M. F. & Pekosz, A. The influenza A virus M2 cytoplasmic tail is required for infectious virus production and efficient genome packaging. *J Virol* **79**, 3595-3605, doi:10.1128/JVI.79.6.3595-3605.2005 (2005).
46 Iwatsuki-Horimoto, K. *et al.* The cytoplasmic tail of the influenza A virus M2 protein plays a role in viral assembly. *J Virol* **80**, 5233-5240, doi:10.1128/JVI.00049-06 (2006).
47 McCown, M. F. & Pekosz, A. Distinct domains of the influenza a virus M2 protein cytoplasmic tail mediate binding to the M1 protein and facilitate infectious virus production. *J Virol* **80**, 8178-8189, doi:10.1128/JVI.00627-06 (2006).
48 Chen, B. J., Leser, G. P., Jackson, D. & Lamb, R. A. The influenza virus M2 protein cytoplasmic tail interacts with the M1 protein and influences virus assembly at the site of virus budding. *J Virol* **82**, 10059-10070, doi:10.1128/JVI.01184-08 (2008).
49 Wang, D. *et al.* The lack of an inherent membrane targeting signal is responsible for the failure of the matrix (M1) protein of influenza A virus to bud into virus-like particles. *J Virol* **84**, 4673-4681, doi:10.1128/JVI.02306-09 (2010).
50 Rossman, J. S. *et al.* Influenza virus m2 ion channel protein is necessary for filamentous virion formation. *J Virol* **84**, 5078-5088, doi:10.1128/JVI.00119-10 (2010).
51 Burleigh, L. M., Calder, L. J., Skehel, J. J. & Steinhauer, D. A. Influenza a viruses with mutations in the m1 helix six domain display a wide variety of morphological phenotypes. *J Virol* **79**, 1262-1270, doi:10.1128/JVI.79.2.1262-1270.2005 (2005).
52 Elleman, C. J. & Barclay, W. S. The M1 matrix protein controls the filamentous phenotype of influenza A virus. *Virology* **321**, 144-153, doi:10.1016/j.virol.2003.12.009 (2004).
53 Bruce, E. A., Digard, P. & Stuart, A. D. The Rab11 pathway is required for influenza A virus budding and filament formation. *J Virol* **84**, 5848-5859, doi:10.1128/JVI.00307-10 (2010).
54 Orenstein, J. M., Meltzer, M. S., Phipps, T. & Gendelman, H. E. Cytoplasmic assembly and accumulation of human immunodeficiency virus types 1 and 2 in recombinant human colony-stimulating factor-1-treated human monocytes: an ultrastructural study. *J Virol* **62**, 2578-2586 (1988).
55 Raposo, G. *et al.* Human macrophages accumulate HIV-1 particles in MHC II compartments. *Traffic* **3**, 718-729 (2002).
56 Pelchen-Matthews, A., Kramer, B. & Marsh, M. Infectious HIV-1 assembles in late endosomes in primary macrophages. *J Cell Biol* **162**, 443-455, doi:10.1083/jcb.200304008 (2003).
57 Jouvenet, N. *et al.* Plasma membrane is the site of productive HIV-1 particle assembly. *PLoS Biol* **4**, e435, doi:10.1371/journal.pbio.0040435 (2006).
58 Finzi, A., Orthwein, A., Mercier, J. & Cohen, E. A. Productive human immunodeficiency virus type 1 assembly takes place at the plasma membrane. *J Virol* **81**, 7476-7490, doi:10.1128/JVI.00308-07 (2007).
59 Deneka, M., Pelchen-Matthews, A., Byland, R., Ruiz-Mateos, E. & Marsh, M. In macrophages, HIV-1 assembles into an intracellular plasma membrane domain containing the tetraspanins CD81, CD9, and CD53. *J Cell Biol* **177**, 329-341, doi:10.1083/jcb.200609050 (2007).
60 Chu, H. *et al.* Tetherin/BST-2 is essential for the formation of the intracellular virus-containing compartment in HIV-infected macrophages. *Cell Host Microbe* **12**, 360-372, doi:10.1016/j.chom.2012.07.011 (2012).

673 61 Welsch, S., Groot, F., Kräusslich, H. G., Keppler, O. T. & Sattentau, Q. J.
674 Architecture and regulation of the HIV-1 assembly and holding compartment in
675 macrophages. *J Virol* **85**, 7922-7927, doi:10.1128/JVI.00834-11 (2011).
676 62 Jouve, M., Sol-Foulon, N., Watson, S., Schwartz, O. & Benaroch, P. HIV-1 buds
677 and accumulates in "nonacidic" endosomes of macrophages. *Cell Host Microbe*
678 **2**, 85-95, doi:10.1016/j.chom.2007.06.011 (2007).
679 63 Hammonds, J. E. *et al.* Siglec-1 initiates formation of the virus-containing
680 compartment and enhances macrophage-to-T cell transmission of HIV-1. *PLoS*
681 *Pathog* **13**, e1006181, doi:10.1371/journal.ppat.1006181 (2017).
682 64 Inlora, J., Chukkapalli, V., Bedi, S. & Ono, A. Molecular Determinants Directing
683 HIV-1 Gag Assembly to Virus-Containing Compartments in Primary
684 Macrophages. *J Virol* **90**, 8509-8519, doi:10.1128/JVI.01004-16 (2016).
685

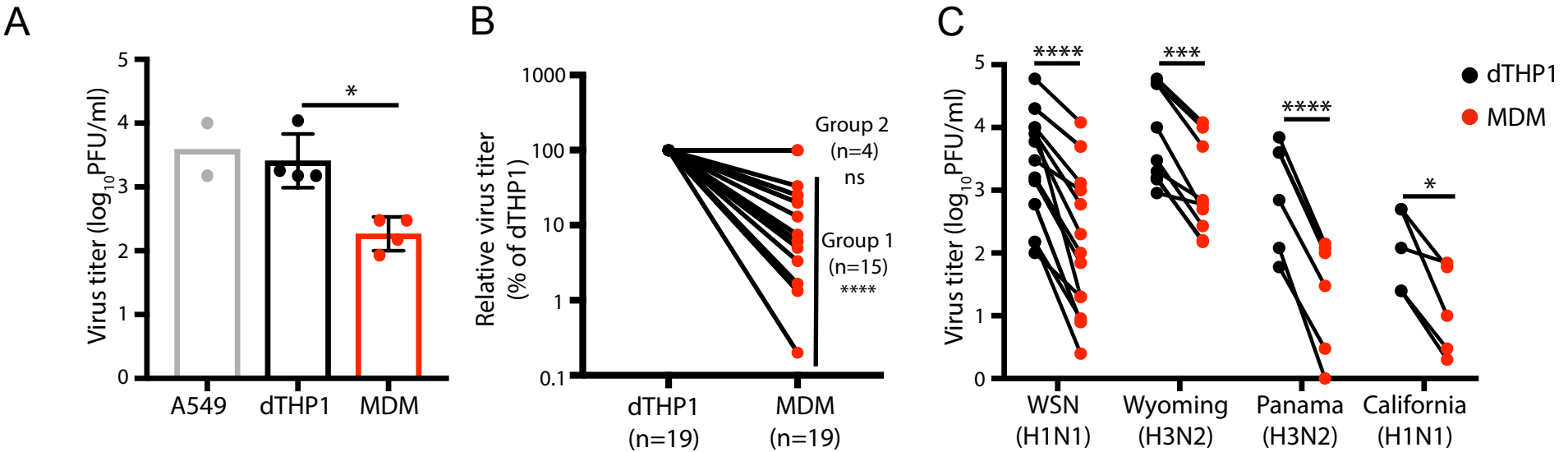

Figure 1: MDM are defective in productive IAV infection. (A) A549, dTHP1 cells and MDM were infected with WSN at MOI 0.01. Infectious virus titers in culture supernatants were measured at 11 hpi. (B) Infectious virus titers in culture supernatants were measured for WSN-infected dTHP1 cells and MDM at 24 hpi. The relative virus titers in MDM cultures were calculated in comparison to the titer in dTHP1 cell cultures tested in each experiment for all tested donors (groups 1 and 2). (C) dTHP1 and MDM (group 1) were infected with the given IAV strains at MOI 0.01, and infectious virus titers in culture supernatants were measured 24 hpi. Each square represents an independently prepared culture. For panel A, data are shown as mean +/- SD. *, P<0.05; **, P<0.01; ***, P<0.001; ****, P<0.0001; ns, non-significant.

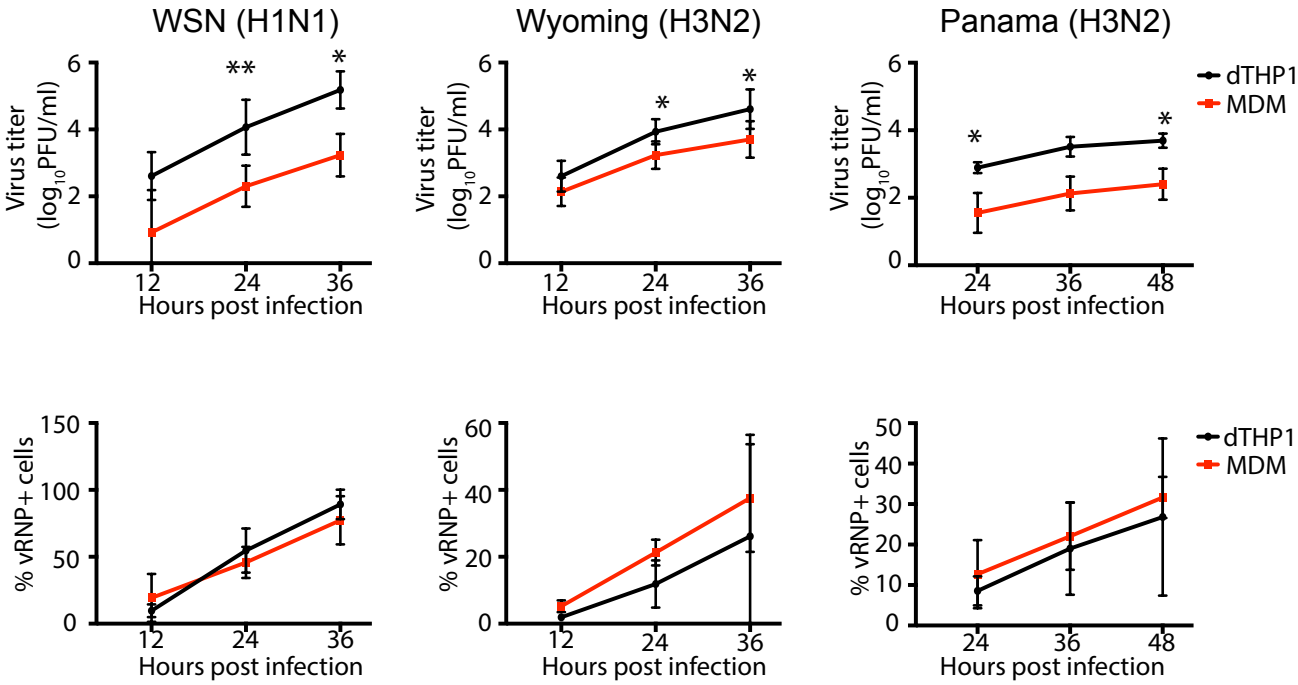

Figure 2: Infectious virus release is reduced in MDM cultures relative to dTHP1 cells despite similar number of infected cells in both cultures. dTHP1 cells and MDM were infected with given IAV strains at MOI 0.01. At the indicated time points post infection, culture supernatants and cells were collected and assessed for virus titer (top panels) and % vRNP+ cells (lower panels), respectively. Data from at least three independent experiments are shown as mean +/- SD. *, P<0.05; **, P<0.01.

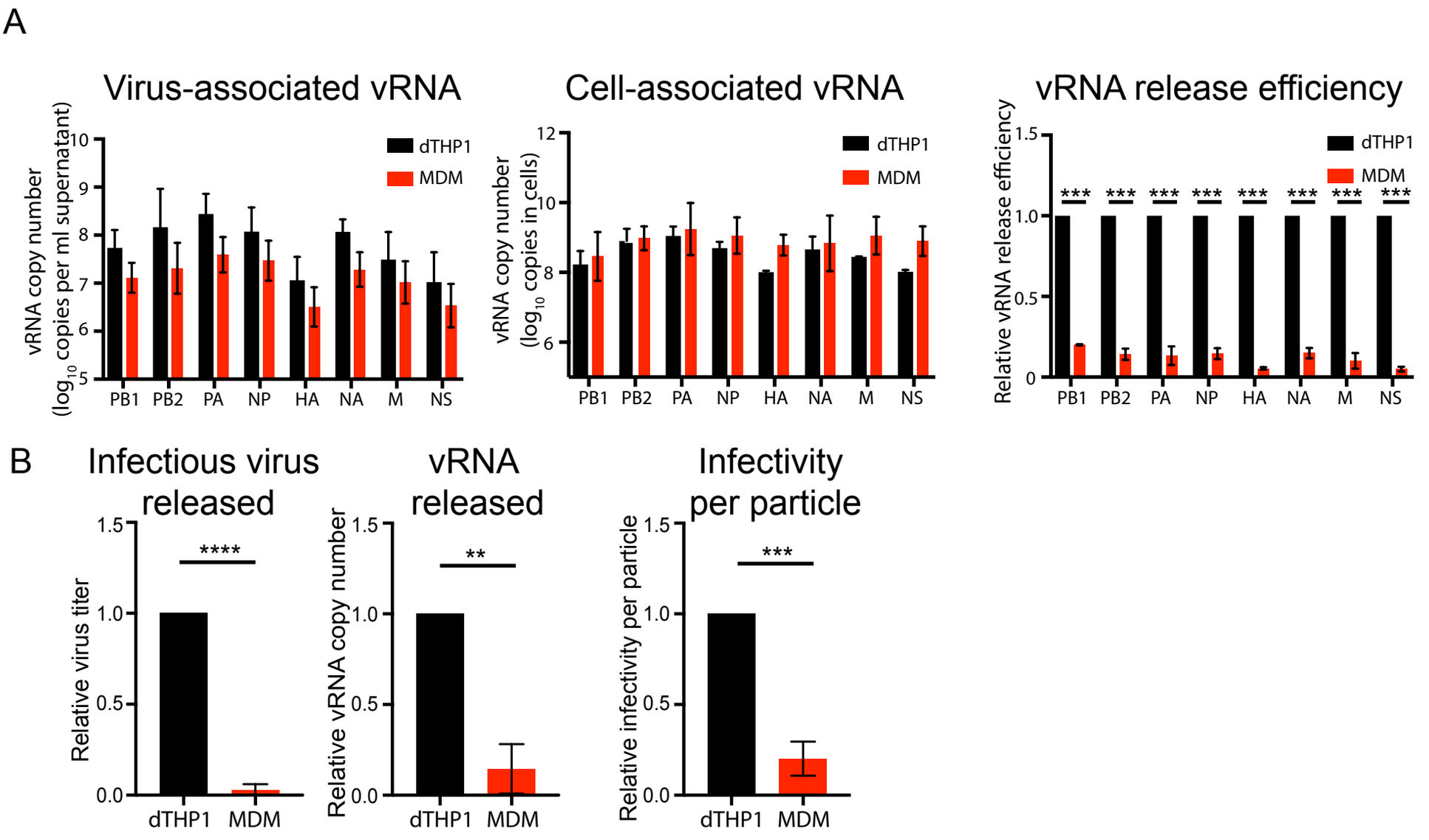

Figure 3: Both efficiency of virus release and infectivity of released particles are reduced in MDM than in dTHP1 cells. dTHP1 cells and MDM were infected with WSN at MOI 0.1. (A) vRNA copy numbers were measured in cell culture supernatants and cell lysates at 20 hpi. vRNA release efficiency was calculated as the ratio of number of vRNA copies in culture supernatants versus total number of vRNA copies (cells+supernatant) for each vRNA segment. (B) PB2 vRNA copy number and virus titer were measured in dTHP1 and MDM culture supernatants at 16 hpi. Infectivity per particle was calculated as the ratio of virus titer to PB2 vRNA copy number in culture supernants. Data are from at least three independent experiments and shown as mean +/- S.D. **, P<0.01; ***, P<0.001, ****, P<0.0001.

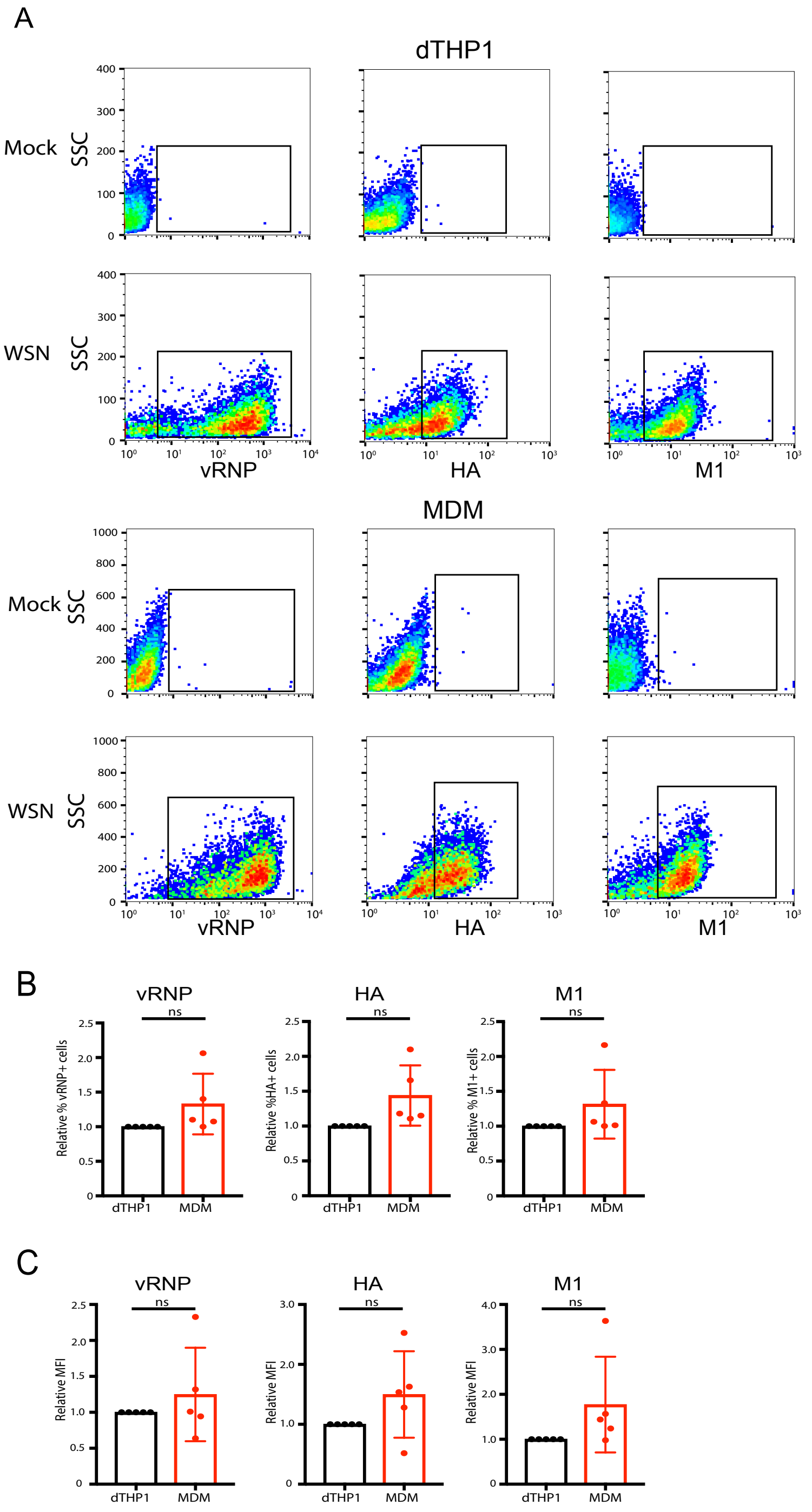

Figure 4: MDM express viral proteins as efficiently as dTHP1 cells. dTHP1 cells and MDM were infected with WSN at MOI 0.01 for 24 hours. Infected cells were fixed, permeabilized and analyzed for cellular levels of vRNP, HA and M1 by flow cytometry. (A) Representative flow plots for mock- and WSN-infected cells are shown. Gates for positive cell populations were set in comparison to mock-infected cells. Due to differences in the side scatter (SSC) profile between dTHP1 cells and MDM, the Y-axis (SSC) range is different between the two cell types. (B) Relative % cells positive (normalized to dTHP1 cells) for vRNP, HA, and M1 are shown. (C) MFIs (normalized to dTHP1 cells) for all three viral components are shown for positive cell populations (gated in panel A) . Data are from at least three independent experiments and are shown as mean +/- SD. ns, non-significant.

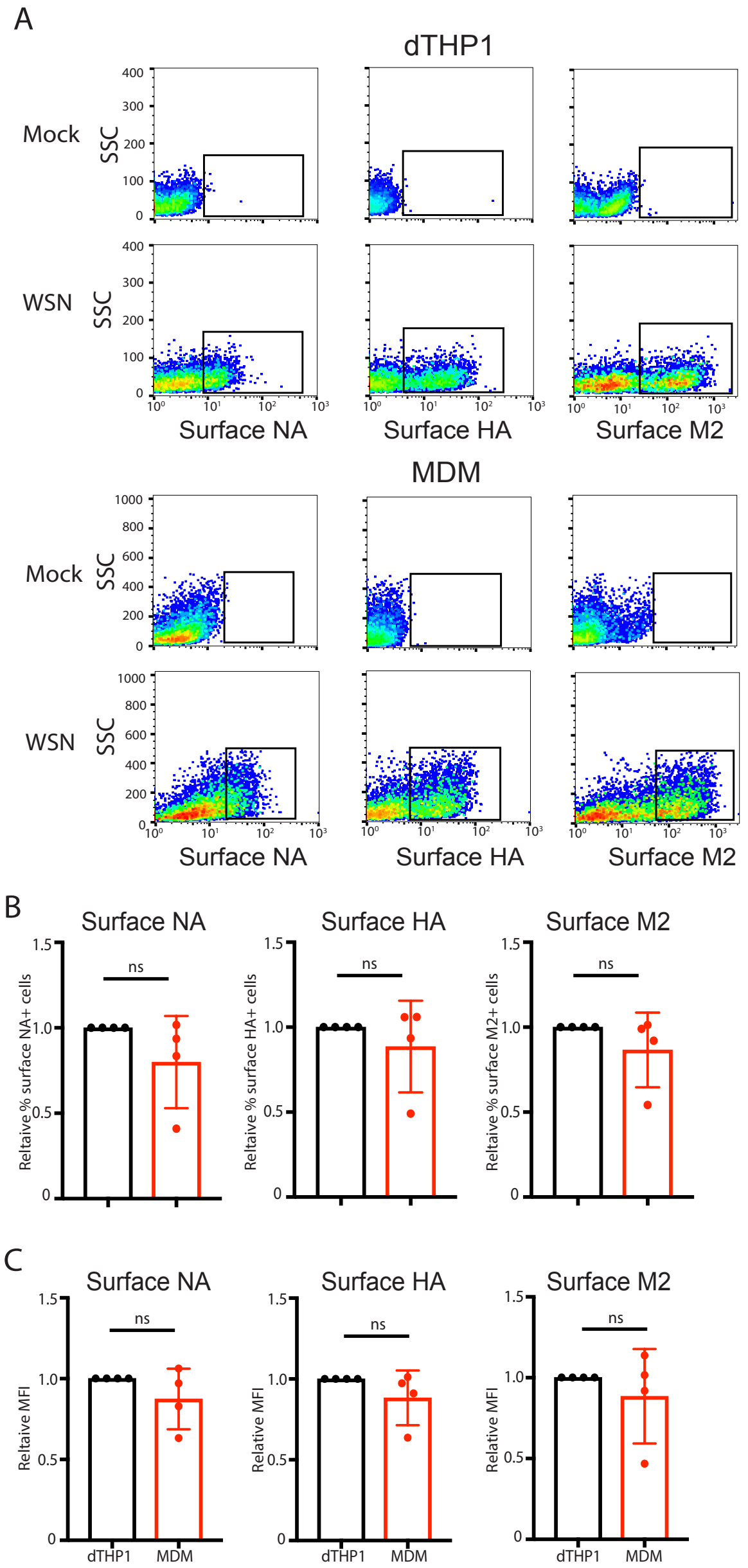

Figure 5: MDM are efficient at trafficking of viral glycoproteins to the cell surface. dTHP1 cells and MDM were infected with WSN at MOI 0.1. (A) Infected cells were analyzed for cell surface expression of HA, NA, and M2 by flow cytometry at 16 hpi. Representative flow plots for mock-infected (top panels) and virus-infected (bottom panels) cells are shown. Due to differences in the side scatter (SSC) profile between dTHP1 cells and MDM, the Y-axis (SSC) range is different between the two cell types.(B) MFI for surface staining of all three proteins is shown as mean +/- SD for positive cell populations. Data are from at least three independent experiments. ns, non-significant

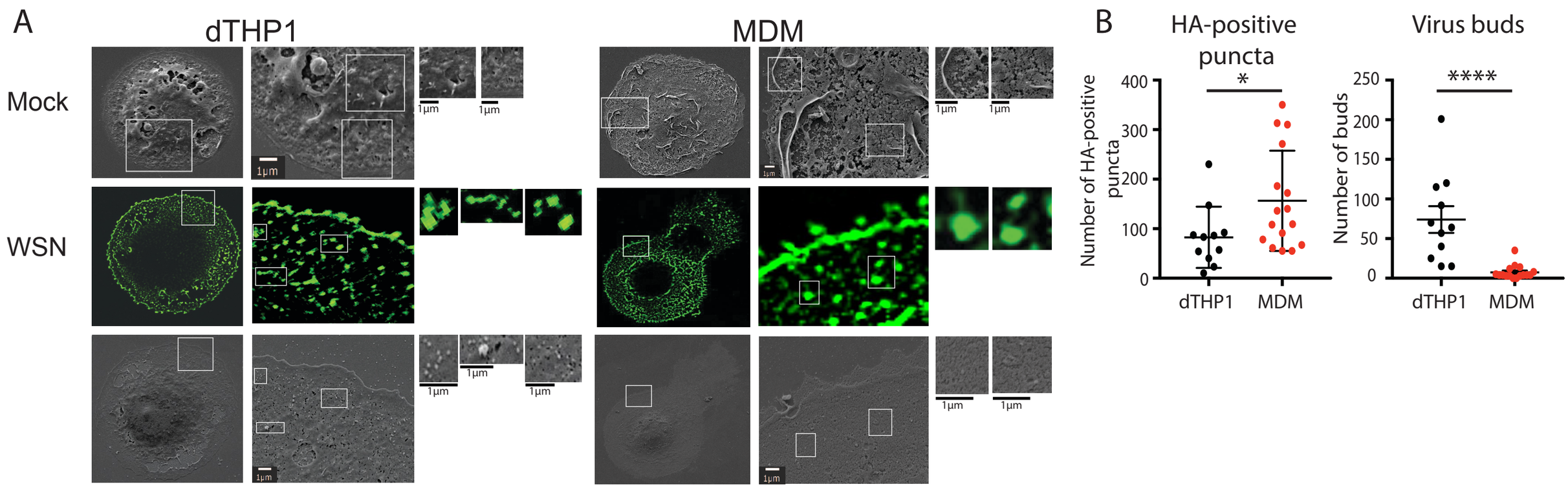

Figure 6: MDM are defective in virus bud formation despite trafficking of HA to the cell surface. dTHP1 cells and MDM were infected with WSN at MOI 0.1. Cells were fixed and immunostained with anti-HA. After identification of HA-positive cells, cells were prepared for SEM. Cells identified to be expressing HA on the cell surface by confocal microscopy were analyzed by SEM. (A) Representative SEM images for mock-infected and WSN-infected HA-positive dTHP1 cells and MDM are shown in the top and bottom rows, respectively. Fluorescence images corresponding to the SEM images of WSN-infected cells are shown in the middle row. Boxed areas are magnified and shown in the right panels. (B) The number of HA-positive puncta (left panel) and virus buds (right panel) were counted within the same area in each cell. Data are shown for 10-20 cells from two independent experiments. Error bars respresent SEM. *, $P<0.05$; ****, $P<0.0001$.

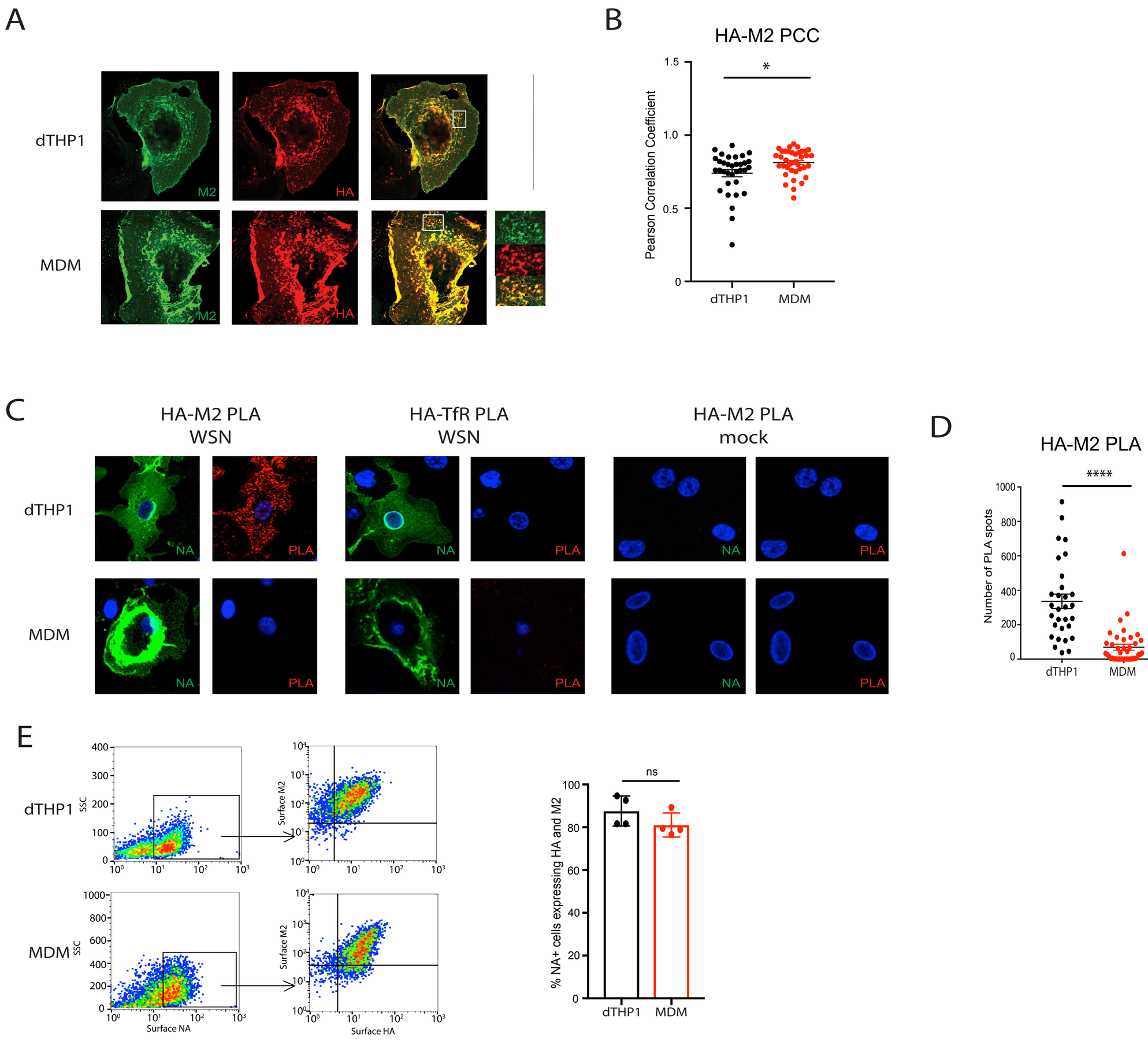

Figure 7: Association between HA and M2 is defective in MDM relative to dTHP1 cells. dTHP1 cells and MDM were infected with WSN. (A) Cells were fixed and stained for surface expressed HA and M2 at 16 or 24 hpi. (B) Pearson correlation coefficient (PCC) for HA and M2 was measured for each cell. (C) Cells were probed with PLA probes and co-stained for surface NA at 16 hpi. Nuclei were stained with DAPI (blue). (D) Number of PLA spots were counted for each cell. For PCC and PLA, 8-10 cells were analyzed per experiment. Error bars represent SEM. (E) % surface NA-positve cells expressing HA and M2 were determined. Representative scatter plots are shown in left panel, and quantified data are shown in the right panel. Data are from at least three experiments and shown as mean +/- SD. *, $p<0.05$; ****, $p<0.0001$; ns, non-significant.